JCI The Journal of Clinical Investigation

Antiviral chemotherapy facilitates control of poxvirus infections through inhibition of cellular signal transduction

Hailin Yang, … , Raymond M. Welsh, Ellis L. Reinherz

J Clin Invest. 2005;115(2):379-387. https://doi.org/10.1172/JCI23220.

Article **Infectious disease**

The EGF-like domain of smallpox growth factor (SPGF) targets human ErbB-1, inducing tyrosine phosphorylation of certain host cellular substrates via activation of the receptor's kinase domain and thereby facilitating viral replication. Given these findings, low molecular weight organic inhibitors of ErbB-1 kinases might function as antiviral agents against smallpox. Here we show that CI-1033 and related 4-anilinoquinazolines inhibit SPGF-induced human cellular DNA synthesis, protein tyrosine kinase activation, and c-Cbl association with ErbB-1 and resultant internalization. Infection of monkey kidney BSC-40 and VERO-E6 cells in vitro by variola strain Solaimen is blocked by CI-1033, primarily at the level of secondary viral spreading. In an in vivo lethal vaccinia virus pneumonia model, CI-1033 alone promotes survival of animals, augments systemic T cell immunity and, in conjunction with a single dose of anti-L1R intracellular mature virus particle-specific mAb, fosters virtually complete viral clearance of the lungs of infected mice by the eighth day after infection. Collectively, these findings show that chemical inhibitors of host-signaling pathways exploited by viral pathogens may represent potent antiviral therapies.

Antiviral chemotherapy facilitates control of poxvirus infections through inhibition of cellular signal transduction

Hailin Yang,[1] Sung-Kwon Kim,[2] Mikyung Kim,[1] Pedro A. Reche,[1] Tiara J. Morehead,[3] Inger K. Damon,[3] Raymond M. Welsh,[2] and Ellis L. Reinherz[1]

[1]Laboratory of Immunobiology, Department of Medical Oncology, Dana-Farber Cancer Institute and Department of Medicine, Harvard Medical School, Boston, Massachusetts, USA. [2]Department of Pathology, University of Massachusetts Medical School, Worcester, Massachusetts, USA. [3]Poxvirus Section, Centers for Disease Control and Prevention, Atlanta, Georgia, USA.

The EGF-like domain of smallpox growth factor (SPGF) targets human ErbB-1, inducing tyrosine phosphorylation of certain host cellular substrates via activation of the receptor's kinase domain and thereby facilitating viral replication. Given these findings, low molecular weight organic inhibitors of ErbB-1 kinases might function as antiviral agents against smallpox. Here we show that CI-1033 and related 4-anilinoquinazolines inhibit SPGF-induced human cellular DNA synthesis, protein tyrosine kinase activation, and c-Cbl association with ErbB-1 and resultant internalization. Infection of monkey kidney BSC-40 and VERO-E6 cells in vitro by variola strain Solaimen is blocked by CI-1033, primarily at the level of secondary viral spreading. In an in vivo lethal vaccinia virus pneumonia model, CI-1033 alone promotes survival of animals, augments systemic T cell immunity and, in conjunction with a single dose of anti-L1R intracellular mature virus particle-specific mAb, fosters virtually complete viral clearance of the lungs of infected mice by the eighth day after infection. Collectively, these findings show that chemical inhibitors of host-signaling pathways exploited by viral pathogens may represent potent antiviral therapies.

Introduction

Chemotherapeutic approaches to the control of viral infections have been less successful than those against bacterial infections because of the need of viruses to replicate in host cells and the attendant difficulty in selectively targeting the virus without damaging the host. To date, virtually all strategies for the development of antiviral drugs have focused on unique properties of the viral replicative cycle or of viral proteins that can be selectively targeted (1–3). These drugs include nucleoside analogues and inhibitors of viral polymerase, protease, and fusion proteins. Most of the antiviral drugs currently in use are directed against persistently infecting viruses, such as HIV, where therapy is expected to continue for a long duration. Acute viral infections, however, may need only a short period of drug treatment to shift the balance between overwhelming and lethal virus load on the one hand and an effective and protective immune response on the other. Because viruses are dependent on host-cell functions for their replication, we questioned whether a transient and well-tolerated interference of the normal functions of the cell types in which the virus replicates may retard viral replication and/or spread and spare the host from morbidity or mortality.

Smallpox was due to infection with variola major or variola minor of the orthopox genus, which belong to the poxvirus family of large double-stranded DNA viruses replicating in the cytoplasm of infected cells (4). Cessation of vaccination efforts more than 2 decades ago has resulted in susceptibility of a large segment of the population to this pathogen (5). This vulnerability requires additional methods to rapidly contain any future outbreak of infections from this group of viruses.

EGF-like growth factors are carried by poxviruses to facilitate viral pathogenesis. Prominent skin manifestations elicited by a number of these viruses are probably linked to this gene product (4). Prior gene deletion studies showed that vaccinia growth factor (VGF) of the variola-related orthopox vaccinia virus (VV) contributes to virulence following intracranial inoculation of mice and intradermal inoculation of rabbits (6). Likewise, inactivation of myxoma growth factor in the distantly related leporipoxvirus diminishes viral-induced proliferation of epithelial cell layers in conjunctival and respiratory tracts (7). Since smallpox growth factor (SPGF) uses ErbB-1 to stimulate host cells (8), thereby aiding viral replication, we reasoned that if the viral factor's stimulatory activity was blocked, then viral growth might be curtailed.

The ErbB 1–4 molecules are members of the receptor tyrosine kinase superfamily and share common structural features, including an extracellular ligand–binding domain, a transmembrane segment, and an intracellular protein tyrosine kinase (PTK) domain (ref. 9 and references therein). These receptors mediate physiologic growth factor signaling by EGF, TGF-α, epiregulin, amphiregulin, and neuregulin, among other growth factors. Although related, there are evident differences in the substrate specificity, signaling properties, and physiology of these receptors. ErbB-2 has no known extracellular ligand, and tyrosine kinase activity is absent in ErbB-3. In addition, heterodimerization and homodimerization of ErbB members contribute to signaling complexity, forming a multilayered network of functional interaction in higher eukaryotes, unlike the single, primordial ErbB homologue found in *Caenorhabditis elegans* and *Drosophila* (9). Since more than 60%

Nonstandard abbreviations used: CAV, cell-associated virus; EEV, extracellular-enveloped virus; IMV, intracellular mature virus; i.n., intranasal(ly); MFI, mean fluorescence intensity; PTK, protein tyrosine kinase; SPGF, smallpox growth factor; VGF, vaccinia growth factor; VV, vaccinia virus; WR, Western Reserve.

Conflict of interest: The authors have declared that no conflict of interest exists.

Citation for this article: *J. Clin. Invest.* **115**:379–387 (2005). doi:10.1172/JCI200523200.

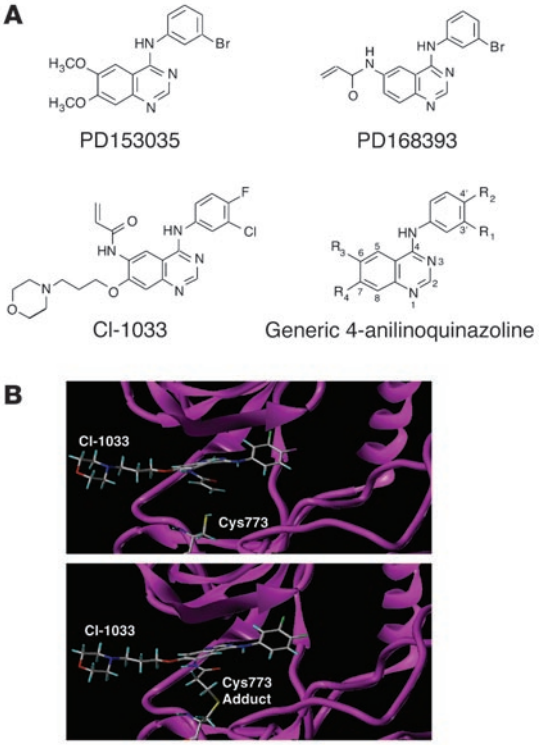

Figure 1
Structure of ErbB tyrosine kinase inhibitors. (**A**) Chemical structures of ErbB tyrosine kinase inhibitors. (**B**) Molecular model of CI-1033 interaction with the ErbB-1 kinase domain. The upper panel shows the model of the noncovalently bound CI-1033 in the ATP-binding site of the tyrosine kinase ErbB-1 (protein data bank: 1M17) crystal structure. The Tarceva compound was removed, and CI-1033 was manually modeled into the site. The backbone of the kinase is shown as a ribbon diagram along with the atoms of Cys773. The lower panel shows the model of the covalently bound CI-1033 in the ATP-binding site. The atoms are shown as stick models with carbon atoms colored white, oxygen atoms red, nitrogen atoms dark blue, sulfur atoms yellow, and hydrogen atoms light blue.

of human tumors contain ErbB abnormalities, including receptor overexpression via gene amplification and/or rearrangement and ErbB receptor–specific ligand aberrations, which contribute to the malignant phenotype (9), approaches have been developed to block ErbB signal transduction. Clinical inhibitors of ErbB receptor tyrosine kinase pathways are being extensively investigated as anticancer agents in many human malignancies (10, 11).

The present study was conducted to determine whether such inhibitors might block orthopox infection and the effects of the EGF-like pathogenic factors in vitro and in vivo. We show here that chemical interference with the signal transduction mediated by ErbB-1 can lead to the control of variola virus in vitro and of VV in vivo. Thus, targeting of a host cell signal transduction function needed for viral replication can be used as a new approach to antiviral chemotherapy.

Results

Identification of the 4-anilinoquinazoline CI-1033 as an inhibitor for SPGF action. Given the high affinity of SPGF for ErbB-1 (K_d = 0.14 nM) (8), we evaluated several tyrosine kinase inhibitors belonging to the 4-anilinoquinazolines that have strong selective specificity for ErbB (Figure 1A). The structure of the ErbB-1 receptor kinase domain alone and in complex with one such inhibitor indicates how these 4-anilinoquinazolines bind to the ATP-binding pocket of the kinase domain (12). Figure 1A shows that PD153035 and PD168393 have an identical 4-(3′-bromo-aniline) ring but differ in the R3 and R4 groups attached to the quinazoline ring. In particular, PD168393 has an acrylamide at position 6 which can alkylate ErbB-1 Cys^{773} so that the inhibitor irreversibly binds to ErbB-1 at a 1:1 M ratio. The tyrosine kinase–active ErbB-2 and ErbB-4 molecules have comparable cysteine residues at Cys^{784} and Cys^{778}, respectively, which can be targeted for modification. In contrast, PD153035 binds in a reversible manner, primarily via hydrophobic forces. CI-1033, like PD168393, has the R3 acrylamide adduct at the 6 position as well as the solubilizing morpholine side chain at the 7 position (R4). CI-1033 demonstrates IC_{50} values of 0.8, 19, and 7 nM for ErbB-1, ErbB-2, and ErbB-4, respectively (13). Figure 1B represents our optimized molecular model for the binding of CI-1033 into the ATP pocket cleft found between the 2 major lobes of the ErbB-1 kinase domain prior to and after formation of the Cys^{773} adduct (14) and is based on the crystal structure of the complex between the ErbB-1 kinase domain and OSI-774, a chemically related 4-anilinoquinazoline (12).

To examine the effects of the 4-anilinoquinazolines on SPGF-triggered activation of human epithelial cells, a series of in vitro experiments was performed. As shown in Figure 2A, after overnight stimulation of human fibroblasts with various concentrations of recombinant SPGF produced and purified as detailed elsewhere (8), the number of cells entering S phase approached 8%. Pretreatment of cells for 1 hour at 37°C with 50 nM concentrations of the indicated inhibitors blocks this increase in DNA synthesis. Figure 2B shows that these same compounds inhibit tyrosine phosphorylation of ErbB-1 (150 kDa band) as well as additional substrates (120 kDa, 80 kDa, 60 kDa, and 55 kDa) triggered by SPGF in HeLa cells. The Src family PTK-specific inhibitor PP2 does not block the phosphorylation of these ErbB-1 substrates even when used at 10 μM. In contrast, addition of PD168393 or CI-1033 at 50 nM largely prevents SPGF-triggered phosphorylation while the effect with PD153035 is only modest at best. These results suggest that reversible inhibitors of kinase activity may be less efficient at blocking substrate tyrosine phosphorylation compared to irreversible inhibitors at the 50 nM concentration tested. Similar inhibition of tyrosine kinase phosphorylation was observed with the vaccinia VGF ortholog (data not shown).

The Figure 2C inset shows the distribution of ErbB-1 receptors in human HeLa epithelial cells prior to or 15 minutes after SPGF addition at 37°C as detected by immunofluorescence microscopy. In the absence of growth factor addition, the distribution of ErbB-1 is primarily confined to the plasma membrane. In contrast, after SPGF exposure, ErbB-1 molecules are rapidly internalized, appearing as punctate intracellular fluorescent aggregates. To assess whether tyrosine kinase inhibitors influence the ability of SPGF to downmodulate ErbB-1, A431 cells were pretreated with inhibitors, incubated with biotinylated SPGF, and shifted to 37°C for 5 minutes; this was followed by fixation. Cell surface-bound ErbB-1 ligand was then visualized with streptavidin-PE and quantitative fluorescence determined by FACS analysis. Without inhibitors, mean fluorescence intensity (MFI) was approximately 110 (Figure 2C). In contrast, the irreversible ErbB inhibitors augmented MFI

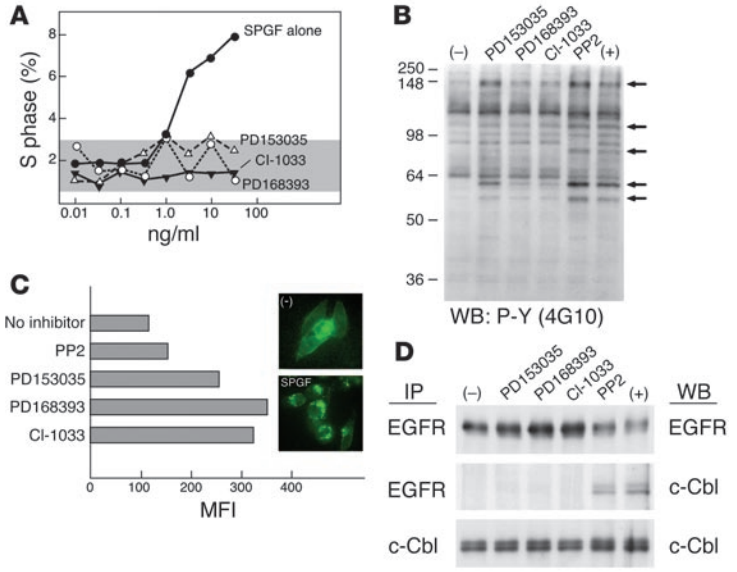

Figure 2

Functional effects of SPGF are blocked by ErbB inhibitors. (**A**) Inhibition of human foreskin fibroblast proliferation by ErbB inhibitors. Human fibroblasts were treated and processed as described in Methods. Percentage of cells entering S phase is plotted. Gray area represents the baseline S phase after serum starvation. (**B**) Inhibitors block cellular protein tyrosine phosphorylation triggered by SPGF. HeLa cells were pretreated with 50 nM inhibitors (PP2, 10 μM) at 37°C for 30 minutes and then stimulated with 50 ng/ml SPGF at 37°C for 15 minutes. Minus (–) indicates no inhibitors or SPGF, and plus (+) indicates SPGF addition only. Total cell lysates were analyzed by Western blotting (WB) with 4G10 anti-phosphotyrosine (P-Y) mAb. Arrows indicate positions of phosphorylated substrates affected by ErbB-1 inhibition. Numbers on left side of the panel indicate the molecular marker in kDa. (**C**) ErbB-1 internalization prevented by inhibitors. A431 cells were pretreated and processed as described in Methods. MFI is recorded by FACS. Results are representative of 3 independent experiments. The inset shows the ErbB-1 cellular distribution pattern in HeLa cells in the absence (–) or presence of SPGF. (**D**) Inhibitors block association of ErbB-1 and c-Cbl and subsequent ErbB-1 degradation. HeLa cells were pretreated with inhibitors and stimulated (37°C, 5 minutes) with SPGF as above. Total cell lysates were immunoprecipitated (IP) with anti-EGFR or anti–c-Cbl and subjected to Western blot with either antibody.

approximately 3-fold (to 300–350) whereas the reversible ErbB-1 inhibitor PD153035 increases MFI to 240. The Src family kinase inhibitor PP2 only modestly affects ErbB-1 surface copy number.

The ErbB receptors are eliminated by 2 pathways: (a) ligand-dependent endocytosis and degradation involving a c-Cbl ubiquitin ligase mechanism (15) and (b) stress-induced shuffling of chaperones associated with these receptors and involving proteasomal proteinases (16). Recent studies show that ErbB-2 kinase inhibition by CI-1033 promotes downregulation of ErbB-2 via the second process (17). However, given that CI-1033 enhances ErbB-1 surface expression, the findings suggest that the effects of CI-1033 on ligand-specific downregulation of ErbB-1 expression are not analogous to those on constitutive ErbB-2 expression. To examine whether 4-anilinoquinazolines might influence c-Cbl interaction with ErbB receptors, inhibitor-pretreated or untreated SPGF-stimulated HeLa cells were immunoprecipitated with anti–ErbB-1 antibodies. Subsequently, Western blotting was performed with either anti–ErbB-1 antiserum to quantitate expression of ErbB molecules or with anti–c-Cbl to assess the effects of the compounds on ErbB-1 association. As shown in Figure 2D, compared to unstimulated cells (–), the SPGF-triggered HeLa cells (+) had less total ErbB-1 due to rapid intracellular degradation. Consistent with what FACS analysis showed (Figure 2C), PP2 had little influence on this process. On the other hand, PD153035, PD168393, or CI-1033 pretreatment augmented the total ErbB-1 protein immunoprecipitated, despite SPGF addition; note the several-fold increase in ErbB-1 (i.e., EGFR) over the SPGF-unstimulated control cells. The latter result implies blockade of constitutive internalization/degradation of ErbB-1 as well. More importantly, SPGF-inducible c-Cbl association with ErbB is blocked by the 4-anilinoquinazolines but not by PP2. Loss of c-Cbl/ErbB-1 complex formation is not secondary to reduction in total cellular c-Cbl levels as shown by parallel c-Cbl immunoprecipitation and Western blotting. Instead, these ErbB kinase inhibitors prevent the inducible association of c-Cbl with ErbB-1 subsequent to SPGF binding.

Effect of CI-1033 on orthopox virus replication and spread. To examine the effect of CI-1033 on variola virus growth, a confluent monolayer of BSC-40 or VERO-E6 monkey kidney epithelial cells was infected with approximately 50 plaque-forming units of variola strain Solaimen in the presence or absence of various concentrations of the ErbB inhibitor and cultured in vitro for 4 days. As shown in Figure 3A of the immmunohistochemical-stained BSC-40 monolayer, increasing concentrations of CI-1033 dramatically reduced the size of the individual plaques and comet formation but had minimal effect on plaque number. This effect is titratable (Figure 3, A–C), and at the highest concentration of 10 μM, extremely small plaques are faintly visible. Although the total number of plaques at the highest concentrations of compound appears to decrease, the difference is not statistically significant ($P > 0.05$) when compared with 7 randomly selected control wells (Figure 3, A and B). Figure 3C illustrates a statistically significant decrease in the number of comets ($P < 0.05$) at CI-1033 concentrations of 500 nM or greater. Comets are representative of extracellular-enveloped virus (EEV) formation and dissemination (15). Similar qualitative observations are made when vaccinia strain IHDJ plaque morphology is observed (see Supplemental Figure 1; supplemental material available online with this article; doi:10.1172/JCI200523220DS1.). A role for VGF is implied by the somewhat smaller plaque size and markedly reduced comet formation observed with the VV growth factor deletion mutant (vSC20, i.e. VGF$^-$) relative to its Western Reserve (WR) parent, as demonstrated on the BSC-40 (see Supplemental Figure 1, inset) and VERO-E6 cells (data not shown). At concentrations of up to 1 μM CI-1033, no effect is observed on the minimal comets made by vSC20, but clear reduction in comet formation is evident for WR (see Supplemental Figure 1, inset).

Consistent with these findings, a single-step growth curve of variola strain Solaimen in VERO-E6 cells demonstrates a delay in EEV formation (see Figure 3D, left panel) and a net reduction in EEV numbers by greater than 2 logs at 10 μM CI-1033. A decrease of less than 1 log in the overall amount of cell-associated virus (CAV) comprising intracellular mature virus (IMV) and cell-associated enveloped viral particles was observed (Figure 3D, right panel). Evaluating single-step growth-curve kinetics in BSC-40 cells demonstrates a less dramatic 1–2 log decrease in EEV with

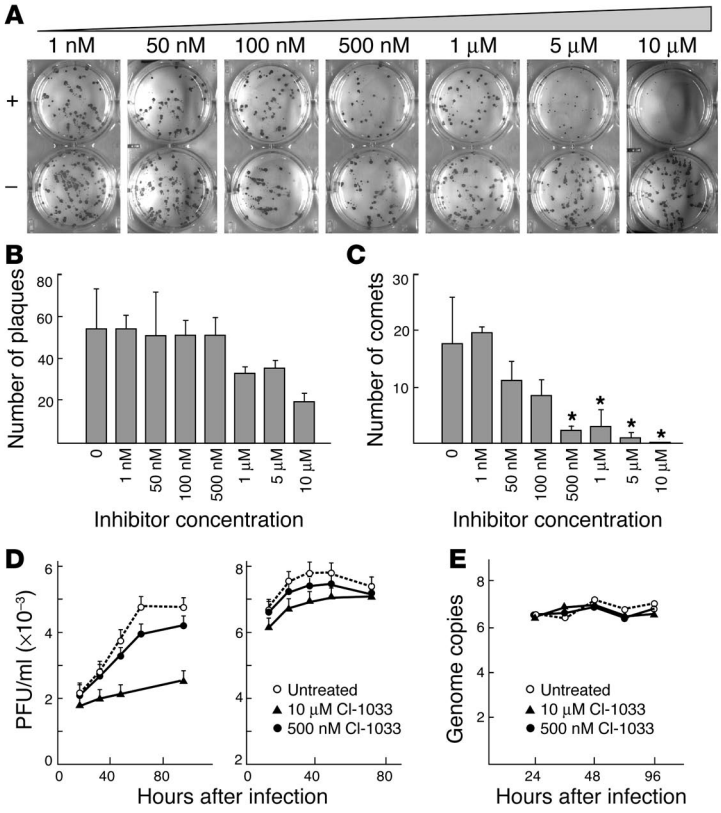

Figure 3
Prevention of secondary variola virus spreading in vitro by ErbB kinase inhibition. (**A**) Immunohistochemical staining of variola strain Solaimen plaques on monolayers of BSC-40 cells after 4 days in the presence (+) or absence (–) of indicated M concentrations of CI-1033. (**B**) Titration effect of CI-1033 on variola plaque formation. (**C**) Titration effect of CI-1033 on variola comet formation. Asterisks indicate statistically significant differences ($P < 0.05$) from 7 randomly selected control wells. (**D**) Time course of variola virus production (single-step growth curve) on VERO-E6 cells in the absence (untreated) or presence of indicated concentration of CI-1033 with left and right panels showing EEV and CAV titers, respectively. (**E**) Viral DNA genome copies from variola single-step growth curve in VERO-E6 cell in the absence (untreated) or presence of 500 nM or 10 μM CI-1033.

10 μM CI-1033 (data not shown). Kinetic evaluation of levels of viral DNA (Figure 3E) in VERO-E6 cells under conditions of high multiplicity infection shows no inhibition of viral DNA accumulation. No evidence of cytotoxicity due to 500 nM or 10 μM CI-1033 was observed in uninfected BSC-40 cells or VERO-E6 cells by either a lactate dehydrogenase assay (see Supplemental Table 1) or trypan blue uptake (data not shown). These aggregate results suggest that CI-1033 does not block primary entry and initiation of viral replication but rather some specific step(s) in viral morphogenesis. Functionally, the release of EEV appears sensitive to inhibition. Orthopox viruses use both microtubule and actin filaments for egress (16, 17) with cell-associated enveloped virus–inducing (CEV-inducing) actin tails to eject themselves from the cell. As ErbB-1 activation reorganizes the actin microfilament system (18), it appears likely that both CEV and EEV release are blocked, retarding secondary virus cell-to-cell spread and hence limiting the size of individual plaques.

Note that the specificity of CI-1033 for ErbB family members is approximately 100,000-fold greater than for unrelated kinases such as PDGF receptor, FGF receptor, insulin receptor, and cyclins D1, A and B (13, 14). This makes a nonspecific effect extremely improbable for doses of CI-1033 that are less than or equal to 1 μM. On the other hand, inhibition of the VGF$^-$ WR variant at the 2 highest drug concentrations (see Supplemental Figure 1, inset) implies either that additional endogenous growth-factor signaling via EGFR is blocked or that inhibition of other viral-egress–relevant tyrosine kinase activation cascades has occurred. By extension, this mechanism(s) applies to vaccinia strains IHDJ and WR and variola viruses. The more profound related effect on long-range dissemination of virus via EEV suggests additional mechanisms of interference. Because EGFR endocytosis is also linked to the actin cytoskeleton (18), ErbB-1 kinase inhibition may serve to maintain surface EGFR expression via this mechanism as well (Figure 2C). More importantly, the ability of CI-1033 to block EGFR activation by cellular ErbB ligands or transstimulation of ErbB-1 via other receptors as well as its downstream effects on cytoskeletal elements used for poxvirus egress likely accounts for the profound effect on plaque morphogenesis not observed with anti-SPGF mAbs (8).

Control of VV infection in vivo by CI-1033. Disruption of the VGF gene in vaccinia WR was shown to reduce pathogenicity of VV in vivo by inhibiting viral growth and shifting the LD_{50} 2,000-fold (6). Since CI-1033 blocks SPGF-stimulated, ErbB-1–driven cell growth, receptor-mediated tyrosine phosphorylation, internalization, and degradation, and in view of its antiviral activity in vitro noted above, we reasoned that the ErbB-1 kinase inhibitor may attenuate orthopox growth factor activity in vivo. To test this possibility, the effect of CI-1033 on the clinical course of B6 mice given an intranasal (i.n.) vaccinia WR challenge (19) was examined. This dose was close to the LD_{50}, so there was some variation in lethality between different experiments with mice of slightly different ages. Figure 4A shows an experiment with 7-week-old mice inoculated with 10^4 PFU in which all (5 of 5) untreated mice died from a fulminant acute pneumonia by day 7 after infection. In contrast, i.p. administration of CI-1033 at 50 mg/kg beginning 6 hours prior to infection and continuing daily for 8 days prevented death for the duration of the experiment. In a second experiment with 9-week-old mice inoculated with 10^4 PFU in which drug treatment was stopped at day 5, 3 of 4 control mice were dead by day 9, but 5 of 5 mice treated with drugs remained alive at day 10, although 3 of 5 succumbed by day 14 (data not shown). In a third experiment with 5-week-old mice receiving 2×10^4 PFU in which drug treatment stopped after 7 days, 4 of 4 untreated and 0 of 5 drug-treated mice died by day 9, 2 of 5 treated mice died at day 10, and 3 of 5 survived for the duration of the experiment (data not shown). These experiments indicate that treatment with the drug alone could consistently either delay or inhibit death in response to this lethal dose of virus. Treatment with a single 200 μg i.p. dose of anti-L1R VV mAb (7D11) known to neutralize the IMV particles could also protect mice from the lethal effects of i.n. inoculation, as could combined anti-L1R and CI-1033 treatment (Figure 4A). Clinical monitoring of animals after infection showed, however, that combined treatment with anti-L1R and CI-1033 reduced symptomatology significantly better than either treatment alone (Figure 4B). The efficacy of combined treatment was further

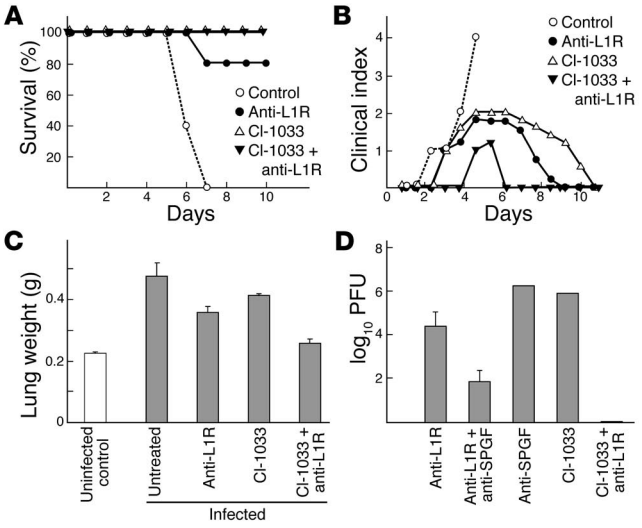

Figure 4
Rescue of mice from lethal vaccinia pneumonia by an ErbB inhibitor. (**A**) Mouse survival curves after i.n. vaccinia inoculation following pretreatment with CI-1033 (1 mg/mouse/day) and/or anti-L1R (200 μg i.p. 6 hours before inoculation). Note that all control mice died by day 7. Each treatment group includes a cohort of 5 animals. (**B**) Clinical score of mice during treatment. The score (0–4) is explained in Methods and is the mean value of the 5 mice per group. (**C**) Average weight of the entire lung 6 days after lethal vaccinia infection with or without indicated treatment (n = 3 per group) versus normal, uninfected lung. (**D**) Virus titers in lungs at day 8 after infection. Results are representative of 5 experiments.

illustrated in an experiment in which 8-week-old mice were given a higher dose of 5×10^4 PFU VV. Mice in all groups died except those with combined therapy, of which 80% (4 of 5) survived.

A cohort of animals was sacrificed at 8 days after infection and their lungs examined. Differences among gross lung weight in each treatment group are shown in Figure 4C. Untreated animals had edematous lungs with multiple hemorrhages, weighing nearly 2 times as much as normal, uninfected B6 lungs. This pathology was somewhat attenuated by anti-L1R or CI-1033 treatment alone but dramatically ameliorated by the combination of CI-1033 and anti-L1R (see Supplemental Figure 2). In 5 experiments, treatment with CI-1033 alone (1 mg/d) only modestly reduced viral lung titers compared to those of untreated infected controls (day 6a, reduced 0.42 $\log_{10}$ PFU; day 6b, reduced 0.14 $\log_{10}$ PFU; day 7, reduced 0.20 $\log_{10}$ PFU; day 8a, reduced 0.08 $\log_{10}$ PFU; day 8b, reduced 0.50 $\log_{10}$ PFU, where a and b refer to independent experiments). This contrasts with the more efficacious anti-L1R in the same experiments (day 6a, reduced 1.1 $\log_{10}$ PFU; day 6b, reduced 0.54 $\log_{10}$ PFU; day 7, reduced 1.2 $\log_{10}$ PFU; day 8a, reduced 2.2 $\log_{10}$ PFU; day 8b, reduced 5.0 $\log_{10}$ PFU). Combined treatment, however, tended to reduce viral titers by greater amounts as shown in these experiments (day 6a, reduced 1.4 $\log_{10}$ PFU; day 6b, reduced 1.3 $\log_{10}$ PFU; day 7, reduced 2.9 $\log_{10}$ PFU; day 8a, reduced 5.1 $\log_{10}$ PFU; day 8b, reduced 5.4 $\log_{10}$ PFU). In these experiments, in which control mice survived, and in another (Figure 4D), in which control mice died, we noted that combined treatment was particularly effective at reducing viral titers by day 7–8 after infection. We have previously observed that mAbs to SPGF that cross-react with VGF can also synergize with anti-L1R to reduce VV lung titers by day 8 (8). Figure 4D shows the enhancing effects of anti-SPGF and of CI-1033 in combination with anti-L1R at 8 days after infection in an experiment in which untreated control animals died and could not be titrated for infectivity (although 7–8 $\log_{10}$ PFU are observed in other experiments). Thus, the CI-1033 drug can apparently replace anti-SPGF mAbs in therapy against VV. The further 2-log viral titer reduction with anti-L1R plus CI-1033 compared with anti-L1R plus anti-SPGF therapy noted in Figure 4D may be a consequence of the irreversible binding of the drug (14) compared with reversible mAb binding, affording a more complete blockade with CI-1033 of the ErbB-1 pathway along with inhibition of endogenous host ErbB ligands. Another explanation may be that CI-1033 blocks dissemination of EEV. In vivo pharmacokinetic studies in mice at the dose range employed herein show peak plasma levels of CI-1033 of 2.2 μM, a concentration inhibiting comet formation in vitro (Figure 3 and data not shown).

We consistently noted that mice treated with CI-1033 alone or in combination with anti-L1R mAb had less morbidity and looked much healthier than non–drug-treated controls, even under conditions in which there were only minor differences in lung viral titers. This may have been due in part to the more effective control of the progression of infection in other organs. In the liver, for example, there were nearly 100-fold lower titers of virus in drug-treated groups by day 5 after infection (day 5, control, 4.6 $\log_{10}$ PFU, vs. drug-treated, 2.8 $\log_{10}$ PFU, P = .02; day 7, control, 4.7 $\log_{10}$ PFU, vs. drug-treated, 3.0 $\log_{10}$ PFU, P = .003). Correspondingly, the number and size of inflammatory foci in the livers were much reduced in the drug-treated mice.

Augmentation of antiviral host response. In the combination anti-L1R plus anti-SPGF immunotherapy model (8), augmented T cell responses to VV were detected by day 6 after infection. To determine whether CI-1033 alone or in combination with anti-L1R may augment T cell responses, we examined T cell–regulated cytokine production in lungs by RNase protection analysis at days 4, 6, and 8 after infection. As shown in Supplemental Figure 3A, compared to what occurred in untreated mice, the use of CI-1033 alone augmented IL-1β, IL-1 receptor antagonist (IL-1Ra), and IFN-γ, peaking at day 6, without influencing IL-6, IL-10, IL-12, or migration inhibitory factor (MIF). For example, the IFN-γ signal was 4.1-fold greater on day 6 with CI-1033–treated mice relative to the control infected animals. Consistent with the lung cytokine level, systemic antigen-specific T cell responses to VV-infected MC57G fibroblasts (H-2^b) were augmented substantially by CI-1033 relative to control untreated mice as judged by splenic $CD8^+CD44^+$ intracellular IFN-γ production (see Supplemental Figure 3B). The percentage of VV-MC57G–activated, IFN-γ–producing $CD8^+$ T cells was 10-fold higher than in untreated VV-infected mice on day 8 after infection; this corresponds to a 21-fold increase in absolute number (1.85×10^5 control cells vs. 8.5×10^3 drug-treated cells). In the same experiment, 23- and 48-fold increases were observed for anti-L1R– and anti-L1R plus CI-1033–treated mice, respectively. That anti-L1R treatment leads to more IFN-γ cytokine RNA in the lung than the anti-L1R plus CI-1033 dual therapy (see Supplemental Figure 3) may be indicative of persistent viral load, particularly at day 8 after infection, with the former treatment (Figure 4D). In sum, chemotherapy alone and combination immunoprophylaxis/chemotherapy are efficient at reducing viral titer and stimulating T cell immunity. The latter may be a consequence of preventing

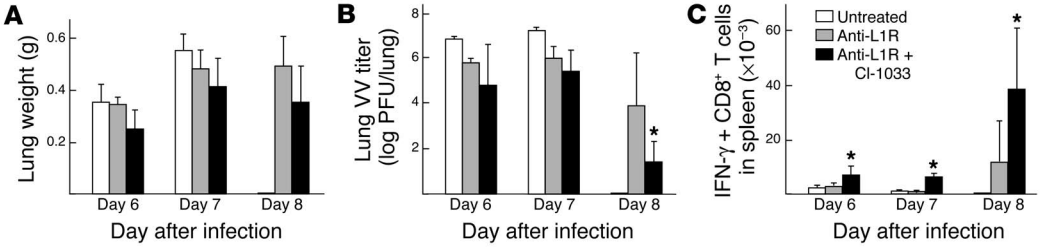

Figure 5

Postexposure therapy of VV infection in the C57BL/6 pneumonia model. Mice were inoculated i.n. with 2×10^4 PFU of VV, and 2 days later were treated with a single dose of mAb L1R or control mAb and/or with CI-1033, the latter given daily until termination of the experiment. Mice were sacrificed on different days after infection and examined for lung weight (**A**), VV PFU/lung (**B**), and the number of anti-CD3–induced IFN-γ–producing $CD8^+$ T cells per spleen (**C**). For days 6, 7, and 8, group sizes of 3–4, 5, or 6 animals, respectively, were employed. At day 8, 2 of 6 anti–L1R-treated mice had undetectable virus, whereas 5 of 6 anti-L1R plus CI-1033–treated mice had undetectable virus. For calculation of mean titers, the lowest detectable titer possible (1 log) was used for mice without detectable virus, such that the means are actually lower values. *$P < 0.05$.

the elaboration of antiinflammatory viral products as well as later rounds of DNA virus replication in epithelial cells dependent on the viral growth factor (20, 21). Given these data, we perceive a linkage between viral growth, viral spreading, and host immunity as modulated through SPGF/VGF and ErbB-1 interaction.

Postexposure therapy. Current interest in orthopox virus therapeutics stems from concerns that variola virus may be used as a bioterrorism agent. Hence, postexposure therapy protocols may be needed as an alternative to postexposure vaccination. We therefore tested the efficacy of CI-1033 as a postexposure therapeutic agent, with and without mAb-dependent immunotherapy. The i.n. VV infection of mice rapidly progresses, unlike the slow incubation time for development of symptoms in humans after exposure to variola (4, 5). Successful therapy in this rapidly progressing VV murine model would thus provide promise for possible drug intervention in human infections. Mice (7–10 weeks of age) were therefore inoculated i.n. with 2×10^4 PFU VV for 2 days to allow for substantial replication of VV, prior to subsequent therapeutic intervention. An initial survival experiment showed that drug treatment alone did not prevent lethality, which was prevented by mAb L1R, with or without CI-1033 (data not shown). Figure 5 summarizes results in 3 other experiments after 4 (day 6), 5 (day 7), and 6 (day 8) days of therapy. Drug treatment alone provided no protection by itself by day 6, though it appeared to augment the protective effect of anti-L1R, in regard to lung weight and lung titers. Those parameters did not reach statistical significance, but by this early time point, a statistically significant increase in anti-CD3–induced IFN-γ–producing $CD8^+$ T cells per spleen was seen with combined therapy. By day 7 the same trends were observed, with combined therapy resulting in lower lung weights and viral titers and now dramatically (6-fold) increased T cell responses. Clinical scores (scoring system as described in Methods and ref. 8) were substantially improved in the combined therapy group at day 7 (untreated, 4.0 ± 0; L1R, 3.4 ± 0.6; L1R plus CI-1033, 2.4 ± 0.5). By day 8, 4 out of 5 of the untreated controls had died, as expected. In comparison to what occurred in L1R-treated mice, there were statistically significant reductions in lung viral titers ($P = 0.02$) in the combined therapy group, which also had reduced lung size, substantial splenomegaly, and more than 3 times the number of VV-specific T cells in the spleen. The heightened T cell response at day 8 allowed for the examination of VV-specific $CD8^+$ T cells, as determined by their production of IFN-γ after incubation with VV-infected DC2.4 dendritic cells. VV-specific T cell responses increased greater than 3-fold in mice receiving combined therapy ($11.4 \pm 3.3 \times 10^5$) compared to those receiving only mAb L1R therapy ($3.2 \pm 4.2 \times 10^5$; $P = 0.002$). These experiments demonstrate the postexposure efficacy of CI-1033 when used in combination with immunotherapy.

Discussion

Recently we characterized SPGF, a protein containing an EGF-like domain that is conserved among orthopox viral genomes, and investigated its possible mechanistic link to skin manifestations associated with smallpox (8). We showed that after recombinant expression, refolding, and purification, the EGF domain of SPGF bound exclusively to the broadly expressed cellular receptor, ErbB-1 (EGFR), with sub-nM affinity, stimulating the growth of primary human keratinocytes and fibroblasts. High-affinity mAbs specific for SPGF revealed in vivo immunoprotection in a murine vaccinia pneumonia model through a mechanism distinct from viral neutralization. These findings suggested that blockade of pathogenic factor actions, in general, may be advantageous to the infected host. Given that ErbB-1 is the host target for SPGF, the possibility that chemical inhibition of ErbB-1 signaling might offer host protection was investigated.

The use of host cellular signaling pathway blockade as a target for antiviral chemotherapy is distinct from other approaches typically directed against pathogens themselves. One advantage of the host-targeted strategy is that drug resistance cannot readily develop. Furthermore, unlike anti-SPGF mAbs (8), where cross-reactivity with other closely related pathogenic factors (i.e., VGF vs. SPGF) is not guaranteed, the ErbB inhibitors are potentially able to block immunologically distinct ligands to various ErbB PTK family members. This broader target activity is relevant since, for example, VGF and myxoma growth factor bind distinct ErbB receptors (22). Whether CI-1033 by itself would be a sufficient therapy against variola virus infection remains to be determined but appears possible given that the dose of orthopox particle inhalation from natural or bioterrorist spread is likely to be less than that employed in the current study, and the time course for the progression of smallpox in humans is much longer than in the VV-infected mouse model. In addition, the drug dosing and scheduling has yet to be optimized. How efficiently postexposure therapy might thwart clinical infection now requires careful scrutiny. That CI-1033 augments T cell responses while reducing infectious symptomatology also suggests its consideration as an immune stimulant postvaccinia vaccination with possible utility in the treatment of complications of immunization. Other ErbB inhibitors (23, 24) may also be useful in this regard.

Aside from poxviruses and their ErbB-directed growth factors, hepatitis B virus and Epstein-Barr virus elaborate factors that dysregulate ErbB-1 transcription (25, 26). RNA tumor viruses also exploit ErbB-1 signaling (27). In addition, functional EGF receptors have been reported to be necessary for efficient reovirus (28) and human cytomegalovirus infection of host cells (29). These findings collectively suggest that multiple viral infections may be coupled to the ErbB-mediated signaling network. Epithelial cells, which constitutively or inducibly express ErbB receptors, are common sites of viral replication (30). Perhaps ErbB inhibitors will have wider application in infectious diseases beyond those involving orthopox viruses. Development of chemical inhibitors of cellular signaling pathways exploited by viral pathogenic factors may offer a new approach toward infectious disease control in general.

Methods

Chemical inhibitors. CI-1033 was provided by Pfizer Inc. PP2, PD153035, and PD168393 were purchased from Calbiochem.

Human fibroblast proliferation assay. Human foreskin fibroblasts (SC-J) were plated in 6-well plates and starved overnight in 2% FCS-DMEM medium, then pretreated with inhibitors for 1 hour at 37°C; this was followed by stimulation with different amounts of SPGF. The cells were harvested 18 hours later and fixed in 80% ice-cold ethanol at 4°C for 1 hour. After a single wash with PBS, cells were stained with 2.5 μg/ml propidium iodide and 50 μg/ml RNase A at 37°C for 30 minutes. Cell cycle data were collected by FACS analysis using Cellquest (BD Biosciences) and analyzed by Modfit (Verity Software House).

ErbB-1 (EGFR) internalization. HeLa cells were cultured on chamber slides and stimulated with ligands (50 ng/ml) at 37°C for 10 minutes. Cells were then fixed using 3.7% formaldehyde for 10 minutes and permeabilized with 0.1% Triton X-100 for 5 minutes at room temperature. Cells were stained with 1 μg of anti-EGFR mAbs (Santa Cruz Biotechnology Inc.) in 1% BSA/PBS at room temperature for 30 minutes; this was followed by staining with anti-mouse Ig-FITC conjugates.

A431 epidermal carcinoma cells were pretreated with 50 nM inhibitors at 4°C for 30 minutes. Biotinylated SPGF (100 ng) was incubated with the cells for a further 30 minutes at 4°C. After washing, cells were incubated at 37°C for 5 minutes and fixed in formaldehyde for 5 minutes at room temperature. Subsequent to streptavidin-PE staining, MFI was obtained by FACS.

Cell lysate preparation, immunoprecipitation, and Western blotting. HeLa cells were treated with 50 nM inhibitors at 37°C for 30 minutes; this was followed by 50 ng/ml SPGF stimulation. Cell lysates were prepared and subjected to immunoprecipitation with anti-EGFR (goat polyclonal; Santa Cruz Biotechnology Inc.) and GammaBind Plus beads (Amersham Biosciences) or anti–c-Cbl beads (Santa Cruz Biotechnology Inc.) at 4°C overnight using previously described methods (8). Beads were washed and eluted in 2× concentration SDS-PAGE–loading buffer and analyzed by Western blotting with either anti-EGFR or anti–c-Cbl.

VV infection of mice. Male C57BL/6 mice aged 4 to 10 weeks were injected i.p. with 200 μg anti-L1R (7D11) mAb in PBS and/or 50 mg/kg/d CI-1033 in 0.05 N sodium lactate buffer, pH 4. Infected control mice were either treated with a control mAb in PBS or sodium lactate buffer without drug. Six hours later, mice were infected i.n. with 4×10^4 PFU VV, WR strain. Each day the mice were weighed and observed for symptoms of infection (0 = normal, 1 = ruffled fur; 2 = 1 plus hunched position; 3 = 2 plus little locomotion; 4 = 3 plus lethargy and minimal response). Virus titer was determined by plaque assay on VERO cells as previously described (31). CI-1033 treatment was of 6–10 days duration. Intracellular cytokine staining of $CD8^+$ T cells was done as previously described, using either anti-CD3, VV-infected MC57G cells, or VV-infected DC2.4 dendritic cells (obtained from Ken Rock, University of Massachusetts Medical School) to stimulate splenic lymphocytes (8). In some experiments, mice were infected with VV 2 days prior to treatment with mAb and/or CI-1033. All animal experimentation was performed according to Association for Assessment and Accreditation of Laboratory Animal Care (AAALAC)-approved protocols for ethical treatment. The work was approved by the University of Massachusetts Medical School Institutional Animal Care and Use Committee.

Titration effect of CI-1033 on variola plaque and comet formation. Confluent BSC-40 monolayers were pretreated or mock-treated in the presence or absence of CI-1033 in RPMI plus 2% FBS (RPMI-2%) at varying concentrations in triplicate for 30 minutes at room temperature. Seven concentrations of CI-1033 were evaluated; 3 mock-treated controls per each concentration of CI-1033 were used on 7 individual 6-well plates. Monolayers were infected with a suspension of variola strain Solaimen in the presence or absence of CI-1033, such that approximately 50 PFU per well of virus were observed. Plates were incubated at 35°C, 6% CO_2 for 1 hour and rocked at 15 minutes intervals to ensure an even infection of the monolayer. The inoculum was removed, and the monolayer was rinsed 1 time with RPMI-2%. The monolayers were overlaid with medium ± CI-1033 at the appropriate concentrations and incubated at 35°C, 6% CO_2 for 4 days. The plates were then γ-irradiated at the kill dose (4.4×10^6 rad) and removed from the Biosafety Level 4 laboratory for immunohistochemical staining. Plaques were immunohistochemically stained for analysis. Comets were defined as 2 or more successively smaller plaques in comet-shaped association with a large plaque. The number of plaques and comets in the presence of different concentrations of CI-1033 was compared to that in control plates using a Wilcoxon rank-sum test. Seven randomly selected mock-treated wells, 1 selected from each of 7 plates, were used for comparison.

Molecular modeling. CI-1033 was docked into the ATP-binding site of the kinase crystal structure (12) manually, based on the information that the compound bound irreversibly to Cys773 (14). The modeling was performed with the Sybyl molecular modeling package using the standard (Maximin) minimizer with the Tripos force field; hydrogen atoms were included, and minimizations were done without charges on any atoms (Tripos). The quinazoline ring of CI-1033 was placed in the same orientation and docking mode as observed for Tarceva, another ErbB inhibitor (12). Distance constraints from the quinazoline N1 to the Met769 backbone NH kept these atoms within hydrogen-bonding distance. Also, distance constraints kept the C2 hydrogen of the quinazoline ring and the carbonyl oxygen of Gln760 to the distance observed in the crystal structure. Torsional constraints were employed to keep the core ring fully planar. CI-1033 was manually placed in the ATP-binding site and the complex minimized, first with the protein aggregated to allow the ligand to fit the pocket after manual docking, then with the constraints removed and minimized for 400 interations.

For the covalently bound variant, the initial modeling of the noncovalently bound variant was the starting point. The sidechain of the CI-1033 molecule was oriented close to the Cys773 sulfur and the appropriate bond formed. All atoms but the ligand and the Cys773 were formed into an aggregate, and the system was minimized. This allowed only the ligand and Cys773 atoms to move. After minimization with the aggregate, the aggregate was removed, and the full system was allowed to minimize for 400 iterations, still maintaining the distance and torsional constraints.

RNase protection assay. One lobe of lung from each treated mouse at various days after infection was disrupted in RLT buffer (QIAGEN) through an 18-gauge needle. Lysates were further homogenized by QIAshredder modules and purified using an RNeasy Mini Kit according to the manufacturer's protocol (QIAGEN). Equal amounts of total RNA (2 μg/mouse) were pooled from 3 mice at each time point (days 4, 6, and 8). Six μg were hybridized and processed with probes made from the mCK-2b template set according to the manufacturer's protocol (BD Biosciences — Pharmingen).

Variola single-step growth curve in BSC-40 and VERO-E6 cells. Confluent BSC-40 and VERO-E6 monolayers were pretreated or mock-treated in the presence or absence of CI-1033 in RPMI-2% FBS at 500 nM and 10 μM concentrations for 30 minutes at room temperature. Monolayers were infected at a MOI of 10 with a suspension of variola strain Solaimen in the presence or absence of CI-1033 at the appropriate concentrations. Plates were incubated at 35°C, 6% CO_2 for 1 hour and rocked at 15-minute intervals to ensure even infection of the monolayer. The inoculum was removed, and the monolayer was rinsed twice with RPMI-2%. The monolayers were overlaid with media ± CI-1033 at the appropriate concentrations and incubated at 35°C, 6% CO_2. EEV and CAV were harvested from independent wells in triplicate at various time points after infection.

Titrating harvested samples. EEV was harvested by removing a 100-μl aliquot of the infection supernatant and serially diluting in 900 μl RPMI-2% plus IMV-neutralizing J2D5 mAbs (1:1000). This concentration of mAbs was demonstrated to neutralize 99% of IMV. Dilutions were then plated onto confluent VERO-E6 cell monolayers and incubated at 35°C, 6% CO_2 for 1 hour and rocked at 15-minute intervals to ensure even infections of the monolayer. The inoculum was removed and the monolayers were overlaid with 2 ml RPMI-2% plus J2D5 mAb. Plates were incubated at 35°C, 6% CO_2 for 4 days and counterstained with Crystal Violet (Sigma-Aldrich) to quantitative plaques. Viral titer was determined by counting plaques. CAV was harvested by removing the remaining infection supernatant after EEV harvest and adding 1 ml fresh RPMI-2% to each well. The CAV samples were then titrated using a standard method for orthopox plaque assay (32). A 1-ml aliquot was placed into a labeled tube and stored at –80°C until titration.

Viral DNA load. Viral DNA was isolated from CAV time point samples using a slight variation of the Bio-Rad Genomic DNA Isolation Protocol (Bio-Rad Laboratories Inc.). Viral DNA load was determined using a real-time PCR method that targets the orthopox virus DNA polymerase.

Cytotoxicity assay. A confluent BSC-40 or VERO-E6 cell monolayer was grown in a 6-well plate and treated with various concentrations of CI-1033 in 2 ml RPMI-2%. The plate was incubated at 37°C, 6% CO_2 for 48 hours. Media were removed from the cell monolayers and placed into corresponding labeled tubes, and an additional 2 ml RPMI-2% was added to each well. Using a 1-cc syringe barrel, cell monolayers were scraped into suspension and then removed to labeled tubes. The cell resuspension samples were lysed using the freeze/thaw method, followed by centrifugation of all samples collected at 250 × *g* for 5 minutes. Cytotoxicity was measured using the CytoTox 96 Non-Radioactive Cytotoxicity Assay Kit and protocol (Promega Corp.). Absorbance was read at 490 nM and percent cytotoxicity was determined and expressed as the amount of experimental lactate dehydrogenase (LDH) released into the medium ± CI-1033 divided by the maximum possible amount of LDH released by lysing of the cells (experimental LDH release/maximum LDH release). Alternatively, after 48 hours, an equal volume of Trypan Blue stain was added to each well. Cells were stained for 10 minutes at room temperature. Stain was removed from the cell monolayer, and cells were observed under a microscope for any evidence of stain absorption, indicating cellular membrane permeability and death.

Online supplemental material. Supplemental Figure 1 shows VV IHDJ comet formation and inhibition by CI-1033 in BSC-40 and VERO-E6 cells. Supplemental Figure 1 inset shows VV WR and VGF deletion mutant (vSC20) comet formation and inhibition by CI-1033 in BSC-40 cells. Supplemental Figure 2 shows hematoxylin and eosin staining of lungs from VV-infected mice in untreated and experimental groups. Supplemental Figure 3 examines whole-lung cytokine expression profiles and IFN-γ production in $CD8^+$ T cells in these groups. Supplemental Table 1 shows minimal to no cytotoxicity of CI-1033 in experiments performed in parallel with the plaque morphology experiments in Supplemental Figure 1. Methods of preparation of rabbit antivariola hyperimmune sera and immunohistochemical staining of variola plaques are given.

Acknowledgments

This work was supported by NIH grants AI57300 and AI19807, a grant from the Dana Foundation (to E.L. Reinherz), and NIH grant AR-35506 (to R.M. Welsh). We thank David Fry, Huifen Chen, and James B. Dunbar for molecular modeling efforts and helpful discussions. We acknowledge scientific input from Miles Brown, Ray Dolin, Wayne Klohs, and Barrett Rollins. We also acknowledge Aaron Curns for statistical support. We thank Bernard Moss for providing WR and vSC20 VV strains. We acknowledge the excellent technical assistance of Keisha Mathurin.

Received for publication August 31, 2004, and accepted in revised form November 23, 2004.

Address correspondence to: Ellis L. Reinherz, Dana-Farber Cancer Institute, 44 Binney Street, Boston, Massachusetts 02115, USA. Phone: (617) 632-3412; Fax: (617) 632-3351; E-mail: ellis_reinherz@dfci.harvard.edu.

Hailin Yang, Sung-Kwon Kim, Mikyung Kim, and Pedro A. Reche contributed equally to this work.

1. Balfour, H.H. 1999. Antiviral drugs. *N. Engl. J. Med.* **340**:1255–1268.
2. Dolin, R. 2001. Antiviral chemotherapy, excluding antiretroviral drugs. In *Principles of Internal Medicine.* 15th edition. E. Braunwald et al., editors. McGraw-Hill. New York, New York, USA. 1092–1100.
3. Fauci, A.S., and Lane, H.C. 2001. Human immunodeficiency virus (HIV) disease: AIDS and related disorders. In *Principles of Internal Medicine*. 15th edition. E. Braunwald et al., editors. McGraw-Hill. New York, New York, USA. 1852–1913.
4. Fenner, F., Wittek, R., and Dumbell, K.R. 1988. *The orthopoxviruses*. Academic Press. San Diego, California, USA. 432 pp.
5. Henderson, D.A., et al. 1999. Smallpox as a biological weapon: Medical and public health management. *JAMA.* **281**:2127–2137.
6. Buller, R.M., Chakrabarti, S., Cooper, J.A., Twardzik, D.R., and Moss, B. 1988. Deletion of the vaccinia virus growth factor gene reduces virus virulence. *J. Virol.* **62**:866–874.
7. Opgenorth, A., Nation, N., Graham, K., and McFadden, G. 1993. Transforming growth factor alpha, Shope fibroma growth factor, and vaccinia growth factor can replace myxoma growth factor in the induction of myxomatosis in rabbits. *Virology.* **192**:701–709.
8. Kim, M., et al. 2004. Biochemical and functional analysis of smallpox growth factor (SPGF) and anti-SPGF monoclonal antibodies. *J. Biol. Chem.* **279**:25838–25848.
9. Yarden, Y., and Sliwkowski, M.X. 2001. Untangling the erbB signalling network. *Nat. Rev. Mol. Cell Biol.* **2**:127–137.
10. Cockerill, G.S., and Lackey, K.E. 2002. Small molecule inhibitors of the class I receptor tyrosine kinase family. *Curr. Top. Med. Chem.* **2**:1001–1010.
11. Wakeling, A.E. 2002. Epidermal growth factor receptor tyrosine kinase inhibitors. *Curr. Opin. Pharmacol.* **2**:382–387.
12. Stamos, J., Sliwkowski, M.X., and Eigenbrot, C. 2002. Structure of the epidermal growth factor receptor kinase domain alone and in complex with a 4-anilinoquinazoline inhibitor. *J. Biol. Chem.* **277**:46265–46272.
13. Allen, L.F., Lenehan, P.F., Eiseman, I.A., Elliott, W.L., and Fry, D.W. 2002. Potential benefits of the irreversible pan-erbB inhibitor, CI-1033, in the treatment of breast cancer. *Semin. Oncol.* **29**:11–21.
14. Fry, D.W., et al. 1998. Specific, irreversible inactivation of the epidermal growth factor receptor and erbB2, by a new class of tyrosine kinase inhibitor. *Proc. Natl. Acad. Sci. U. S. A.* **95**:12022–12027.
15. Soubeyran, P., Kowanetz, K., Symkiewicz, I., Langdon, W.Y., and Dikic, I. 2002. Cb1-CIN85-endophilin complex mediates ligand-induced downregulation of EGF receptors. *Nature.* **416**:183–187.
16. Xu, W., et al. 2001. Sensitivity of mature ErbB2 to geldanamycin is conferred by its kinase domain and is mediated by the chaperone protein Hsp90. *J. Biol. Chem.* **276**:3702–3708.
17. Citri, A., et al. 2002. Drug-induced ubiquitylation and degradation of ErbB receptor tyrosine kinases: implications for cancer therapy. *EMBO J.* **21**:2407–2417.
18. Lynch, D.K., et al. 2003. A Cortactin-CD2-associated protein (CD2AP) complex provides a novel

link between epidermal growth factor receptor endocytosis and the actin cytoskeleton. *J. Biol. Chem.* **278**:21805–21813.
19. Chen, H.D., et al. 2001. Memory CD8+ T cells in heterologous antiviral immunity and immunopathology in the lung. *Nat. Immunol.* **2**:1067–1076.
20. Alcami, A. 2003. Viral mimicry of cytokines, chemokines and their receptors. *Nat. Rev. Immunol.* **3**:36–50.
21. Seet, B.T., et al. 2003. Poxviruses and immune evasion. *Annu. Rev. Immunol.* **21**:377–423.
22. Tzahar, E., et al. 1998. Pathogenic poxviruses reveal viral strategies to exploit the ErbB signaling network. *EMBO J.* **17**:5948–5963.
23. Fry, D.W., et al. 1994. Specific inhibitor of the epidermal growth factor receptor tyrosine kinase. *Science.* **265**:1093–1095.
24. Levitzki, A., and Gazit, A. 1995. Tyrosine kinase inhibition: an approach to drug development. *Science.* **267**:1782–1788.
25. Menzo, S., et al. 1993. Transactivation of epidermal growth factor receptor gene by the hepatitis B virus X-gene product. *Virology.* **196**:878–882.
26. Miller, W.E., Earp, H.S., and Raab-Traub, N. 1995. The Epstein-Barr virus latent membrane protein 1 induces expression of the epidermal growth factor receptor. *J. Virol.* **69**:4390–4398.
27. Adelsman, M.A., Huntley, B.K., and Maihle, N.J. 1996. Ligand-independent dimerization of oncogenic v-erbB products involves covalent interactions. *J. Virol.* **70**:2533–2544.
28. Strong, J.E., Tang, D., and Lee, P.W.K. 1993. Evidence that the epidermal growth factor receptor on host cells confers reovirus infection efficiency. *Virology.* **197**:405–411.
29. Wang, X., Huong, S.-M., Chiu, M.L., Raab-Traub, N., and Huang, E.-S. 2003. Epidermal growth factor receptor is a cellular receptor for human cytomegalovirus. *Nature.* **424**:456–461.
30. Yoo, J.-Y., and Desiderio, S. 2003. Innate and acquired immunity intersect in a global view of the acute-phase response. *Proc. Natl. Acad. Sci. U. S. A.* **100**:1157–1162.
31. Selin, L.K., Varga, S.M., Wong, I.C., and Welsh, R.M. 1998. Protective heterologous antiviral immunity and enhanced immunopathogenesis mediated by memory T cell populations. *J. Exp. Med.* **188**:1705–1715.
32. Earl, P.L., Cooper, N., Wyatt, L.S., Moss, B., and Carroll, M.W. 2004. Preparation of cell cultures and vaccinia virus stocks. In *Current Protocols in Molecular Biology.* F.M. Ausubel et al., editors. John Wiley & Sons. New York, New York, USA. 16.16.